Versatile Preparation of Silica Nanocapsules for Biomedical Applications

Shuai Jiang, Milagro Mottola, Shen Han, Raweewan Thiramanas, Robert Graf, Ingo Lieberwirth, Volker Mailänder, Daniel Crespy,* and Katharina Landfester*

Core–shell nanocapsules are receiving increasing interest for drug delivery applications. Silica nanocapsules have been the focus of intensive studies due to their biocompatibility, versatile silica chemistry, and tunable porosity. However, a versatile one-step preparation of silica nanocapsules with well-defined core–shell structure, tunable size, flexible interior loading, and tailored shell composition, permeability, and surface functionalization for site-specific drug release and therapeutic tracking remains a challenge. Herein, an interfacially confined sol–gel process in miniemulsion for the one-step versatile preparation of functional silica nanocapsules is developed. Uniform nanocapsules with diameters from 60 to 400 nm are obtained and a large variety of hydrophobic liquids are encapsulated in the core. When solvents with low boiling point are loaded, subsequent solvent evaporation converts the initially hydrophobic cavity into an aqueous environment. Stimuli-responsive permeability of nanocapsules is programmed by introducing disulfide or tetrasulfide bonds in the shell. Selective and sustained release of dexamethasone in response to glutathione tripeptide for over 10 d is achieved. Fluorescence labeling of the silica shell and magnetic loading in the internal cavity enable therapeutic tracking of nanocapsules by fluorescence and electron microscopies. Thus, silica nanocapsules represent a promising theranostic nanoplatform for targeted drug delivery applications.

1. Introduction

Multifunctional nanocarriers integrating the properties of bioimaging, targeting, and stimuli-responsive release of guest molecules allow a spatiotemporal controlled delivery and tracking of therapeutics, which is the prime prerequisite for in vivo nanocarrier-mediated drug delivery.[1–4] Driven by the rapid progress in their synthetic control, mesoporous silica nanomaterials have attracted increasing attention due to their large specific surface area, tunable pore volume and structure, and facile surface modification, thus showing a wide application prospect for drug delivery and biomedicine.[5–15] Compared with mesoporous silica nanoparticles with a solid core, core–shell silica nanocapsules (SiO_2 NCs) have the advantages that their interior cavity offers a large loading capacity for guest molecules and the shell can be designed to display a tunable permeability for specific cargo release.[16] In spite of recent progress in nanocapsules design, a versatile approach for the preparation of functional SiO_2 NCs for biomedical applications with control at morphological and molecular levels, e.g., the core–shell structure, tunable size, interior contents, and the shell composition, permeability, and surface functionalization, is still needed.

Hard-templating approaches are often used for preparing SiO_2 NCs as they typically result in well-defined size and shape.[17] For example, redox-triggered biodegradable NCs with disulfide-bridged silsesquioxane frameworks were synthesized by using poly(acrylic acid) nanoaggregates[18] and silica nanoparticles[19] as templates, which were subsequently removed. The payloads were postloaded in the hollow

Dr. S. Jiang, M. Mottola, S. Han, Dr. R. Thiramanas, Dr. R. Graf,
Dr. I. Lieberwirth, Prof. V. Mailänder, Prof. D. Crespy, Prof. K. Landfester
Max Planck Institute for Polymer Research
Ackermannweg 10, 55128 Mainz, Germany
E-mail: daniel.crespy@vistec.ac.th; landfester@mpip-mainz.mpg.de

M. Mottola
Depto. de Química
Cátedra de Química Biológica
Facultad de Ciencias Exactas
Físicas y Naturales
Universidad Nacional de Córdoba
Av. Vélez Sársfield 1611, X5016GCA Córdoba, Argentina

M. Mottola
CONICET
Instituto de Investigaciones Biológicas y Tecnológicas (IIBYT)
Av. Vélez Sarsfield 1611, X5016GCA Córdoba, Argentina

Prof. V. Mailänder
Dermatology Clinic
University Medical Center of the Johannes Gutenberg-University
Langenbeckstr. 1, 55131 Mainz, Germany

Prof. D. Crespy
Max Planck-VISTEC Partner Laboratory for Sustainable Materials
Department of Materials Science and Engineering
School of Molecular Science and Engineering
Vidyasirimedhi Institute of Science and Technology (VISTEC)
Rayong 21210, Thailand

capsules by adsorption. This strategy often results in low loading efficiency and initial burst release especially for water-soluble molecules.[16,20,21] Alternatively the payloads can be predissolved or adsorbed in the template material. Nonetheless, this approach takes several steps and the loading efficiency of guest molecules relies highly on their adsorption to the template nanoparticles.[16]

Emulsion-based approaches have been widely studied for the encapsulation of payloads in nanocapsules. Guest molecules or particles are first dissolved or dispersed in template liquid droplets, followed by the formation of a surrounding silica shell. A range of materials with different sizes and polarities, such as enzymes,[22,23] corrosion inhibitors,[24,25] self-healing agents,[26] agrochemicals,[27,28] therapeutic agents,[29,30] imaging probes,[31,32] and organic dyes[29,33] were encapsulated in SiO_2 NCs by using water-in-oil or oil-in-water emulsions.[16] Cationic surfactants, such as cetyltrimethylammonium bromide and chloride were often used as templating agents for confining silica formation at droplets interface.[24–26] Wibowo et al. developed a biomimetic templating technique by designing a dual functional peptide by modularizing a surface-active sequence capable of stabilizing oil droplets in water with another sequence for catalyzing biosilicification at oil–water interfaces.[27] This biomineralizing peptide enabled the formation of SiO_2 NCs at near-neutral pH value and ambient temperature. However, the large scale production of complex peptides is a limiting factor.[34,35] Jakhmola et al. synthesized SiO_2 NCs via a biosilicification process induced by poly(l-lysine) immobilized on the surface of emulsion droplets.[36] This synthetic process requires several steps. First, a central oil core was stabilized by a lecithin surfactant, followed by the adsorption of positively charged poly(l-lysine) on the droplets. Afterward, negatively charged silica species were attached onto nanodroplets and formed a silica shell. Erni et al. synthesized microcapsules with dense walls composed entirely of a biopolymer scaffold interpenetrated with amorphous silica.[37] A weakly acidic hydrogel shell was first formed around oil droplets, which then served as a scaffold to induce protein-directed mineralization of silica. The precipitation process, occurring in the hydrogel scaffold, consumed water to form silica, yielding dense shells with a very low permeability for volatile organic compounds. However, the diameter of capsules was hundreds of μm, which is out of the applicability range for in vivo drug delivery via intravenous administration (>>5 μm).[38] Although these synthetic approaches were successful, effective, and versatile synthetic approaches that are independent of customized templating agents and avoid multiple steps are still needed to prepare well-defined SiO_2 NCs for biomedical applications.

In this study, we developed a one-step approach for versatile preparation of functional SiO_2 NCs for biomedical applications. The SiO_2 NCs were synthesized via a confined sol–gel process at the nanodroplet-water interface of oil-in-water miniemulsions (**Figure 1**a). By this approach, a versatile synthesis of SiO_2 NCs with morphological and molecular control was achieved, including a defined core–shell structure, tunable size, flexible interior loading, and tailored shell composition, permeability, and surface functionalization. These features allow site-specific drug release and enable therapeutic tracking of labeled SiO_2 NCs by fluorescence and electron microscopic techniques.
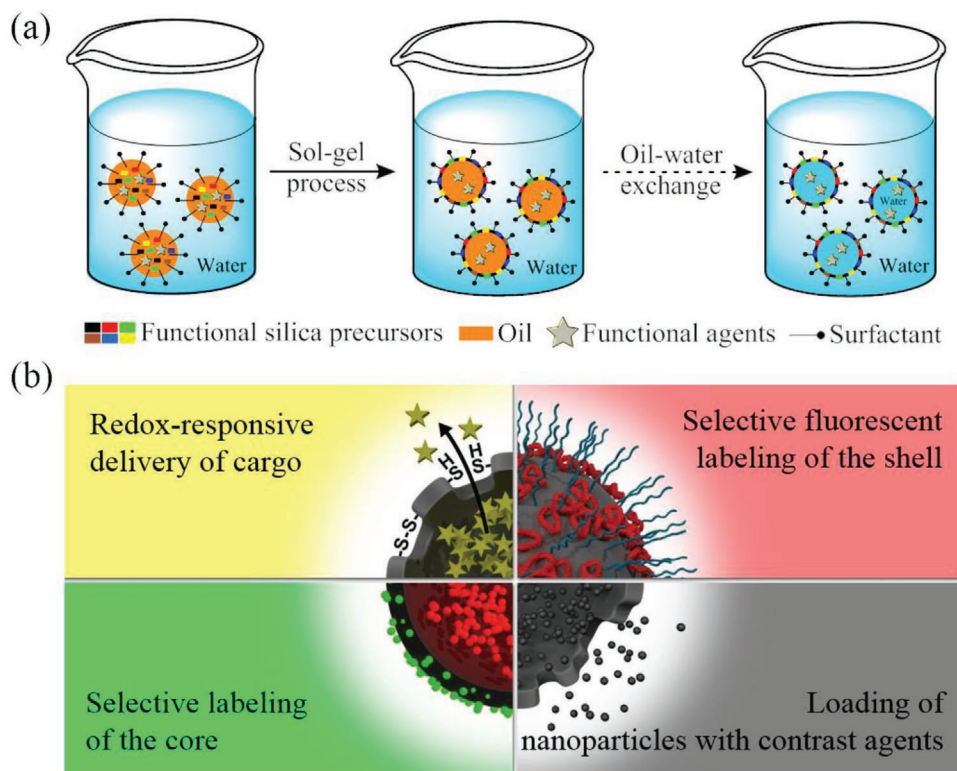
Figure 1. Schematic illustration for: a) The preparation of silica nanocapsules dispersed in water. The initially hydrophobic core can be converted to an aqueous core. b) Features of the silica nanocapsules offered by this synthetic procedure.

**ADVANCED
SCIENCE NEWS**
www.advancedsciencenews.com

Particle
& Particle Systems Characterization
www.particle-journal.com

2. Results and Discussion

The SiO$_2$ NCs were synthesized via a confined sol–gel process at the nanodroplets-water interface in an oil-in-water miniemulsion. The oil phase forming the nanodroplets consisted in a mixture of silica precursors, osmotic pressure agent, organic solvent, and functional payloads to be encapsulated. This hydrophobic mixture was subsequently dispersed in an aqueous solution of surfactant by ultrasonication (see Figure 1a). By this approach, therapeutic agents were directly encapsulated in the liquid core of nanocapsules during the shell formation. Simultaneously, functional silica precursors, i.e., alkoxysilanes containing amino groups, fluorescent probes, or redox-responsive disulfide bonds, can be integrated in the silica shell to achieve multiple control for the morphology, cargo loading, shell composition, and functionality in one step.

2.1. Control of the Core–Shell Structure by Interfacially Confined Silicification

Cetyltrimethylammonium chloride (CTMA-Cl) was used here as a cationic surfactant to stabilize the miniemulsion droplets against coalescence. More importantly, the second role of CTMA-Cl is to serve as templating agent for confining the condensation of hydrolyzed silica precursors at oil/water interface via cooperative self-assembly of negatively charged silica species and cationic surfactant, hence avoiding secondary nucleation of silica in the continuous phase (**Figure 2**a).[16] This electrostatic interaction results from the dissociation of silanol groups at experimental pH (4-5), which is above the isoelectric point of silica (≈pH 2–3).[39] To demonstrate the templating effect generated by CTMA-Cl, we used the nonionic surfactant Lutensol AT50 to fully or partially replace CTMA-Cl (Table S1, Supporting Information). When the nonionic surfactant was used without CTMA-Cl, no capsules were observed by transmission electron microscopy (TEM). Only small nanoparticles were observed (Figure 2b), indicating a noncontrolled nucleation of silica in the continuous phase (Figure 2a). Precipitation of white solids was observed after 24 h storage without stirring (Figure S1a, Supporting Information). When CTMA-Cl was introduced, nanocapsules with defined core–shell structure were observed by TEM (Figure 2c–f). Core–shell nanocapsules were formed at 10% CTMA-Cl. However, gelation of the dispersion was observed after 24 h of storage without stirring (Figure S1b, Supporting Information), which suggests an insufficient confinement of silanol condensation at the droplets' interface. Remarkably, the dispersions were stable when ≥25% CTMA-Cl were used (Figure S1c–e, Supporting Information). The size of the nanocapsules were smaller with increasing amount of CTMA-Cl (Table S1, Supporting Information), which is attributed to the generally higher stabilizing efficiency of low molecular weight cationic surfactants compared with nonionic surfactants.[40]

2.2. Controlling the Size of the Nanocapsules

The size of drug delivery nanocarriers influences their in vivo pharmacokinetics, including cellular uptake, biodistribution, and circulation half-life of nanoparticles.[41] In miniemulsion polymerization, the particle size can be varied in a wide range mainly by changing the type and amount of surfactant. Other factors, such as the volume ratio of
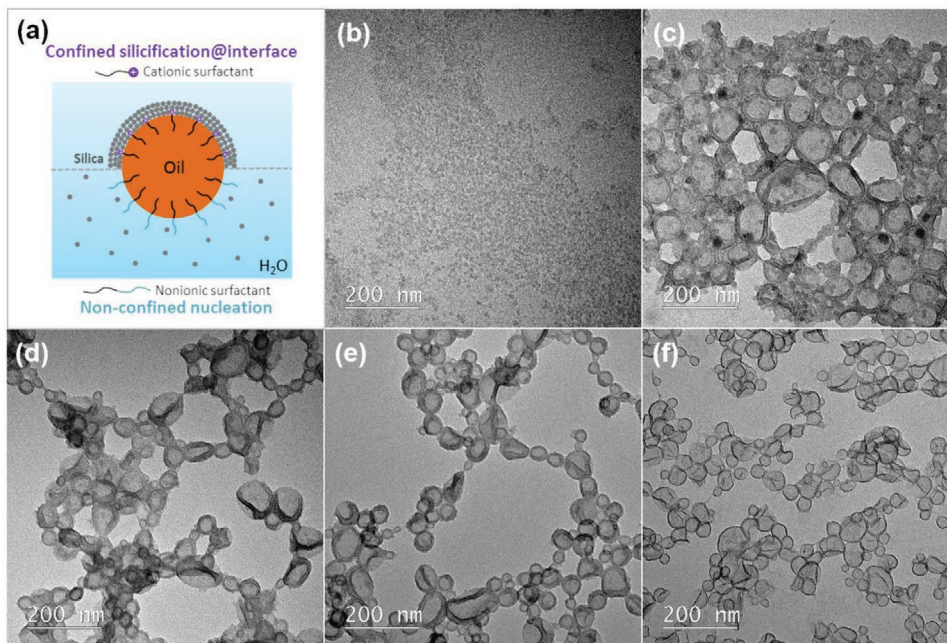
Figure 2. a) Schematic illustration of the confined interfacial silicification process templated by CTMA-Cl. b–f) TEM micrographs of nanocapsules stabilized by mixtures of CTMA-Cl and Lutensol AT50 with $n_{CTMA-Cl}$:$n_{Lutensol}$ molar ratio of b) 0:1 (sample SJP120a), c) 1:22.7 (sample SJP120b), d) 1:7.6 (sample SJP120c), e) 1:2.5 (sample SJP120d), and f) 1:0 (sample SJP120f).

1900484 (3 of 12)
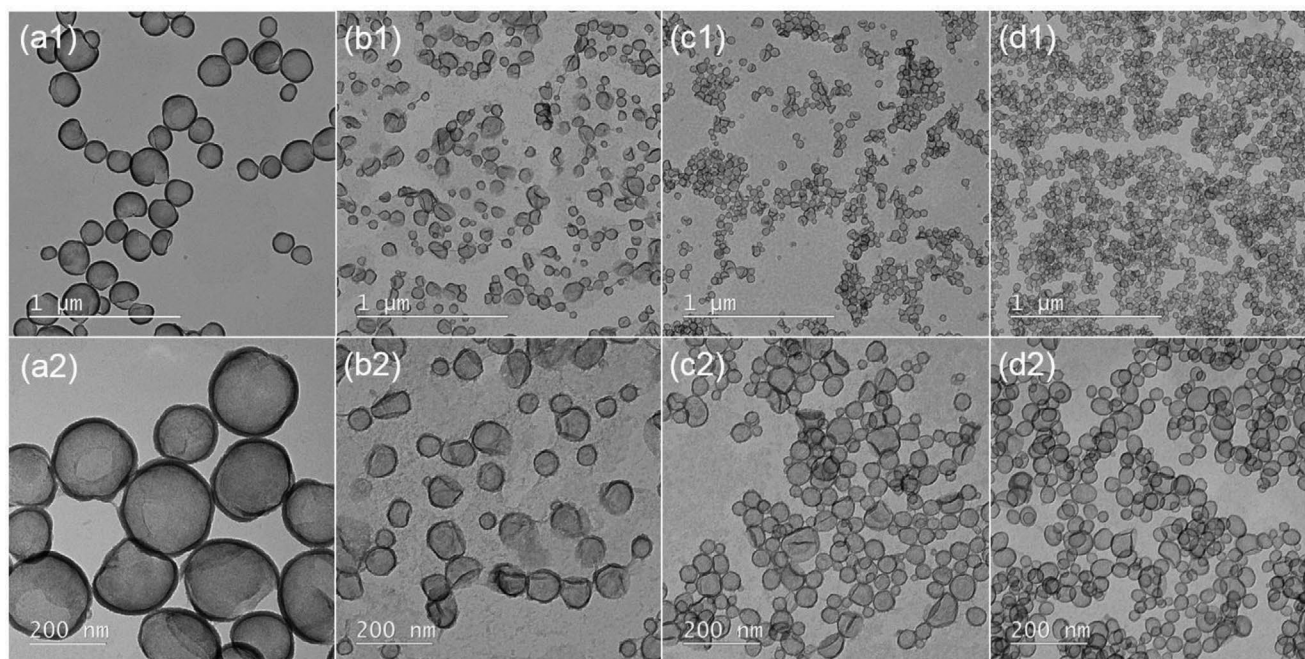
Figure 3. TEM micrographs of SiO_2 NCs with hydrodynamic diameter D_h controlled by tuning the oil/water volume ratio. a) $D_h = 395$ nm, d (shell thickness) $\approx 17 \pm 4$ nm, $V_{oil}/V_{water} = 40\%$ (sample SJP45-0), b) $D_h = 147$ nm, $d \approx 8 \pm 2$ nm, $V_{oil}/V_{water} = 20\%$ (sample SJP45-1), c) $D_h = 103$ nm, $d \approx 5 \pm 2$ nm, $V_{oil}/V_{water} = 10\%$ (sample SJP45-2), and d) $D_h = 59$ nm, $d \approx 4 \pm 2$ nm, $V_{oil}/V_{water} = 5\%$ (sample SJP45-3).

dispersed phase to continuous phase, energy input, and electrolyte concentration of the aqueous phase can also play a role on the particle size.[40] To obtain nanocapsules with a narrow size distribution, an osmotic agent acting as costabilizer is essential for hindering Ostwald ripening of the nanodroplets. Hexadecane was used here due to its very low solubility in water.[42]
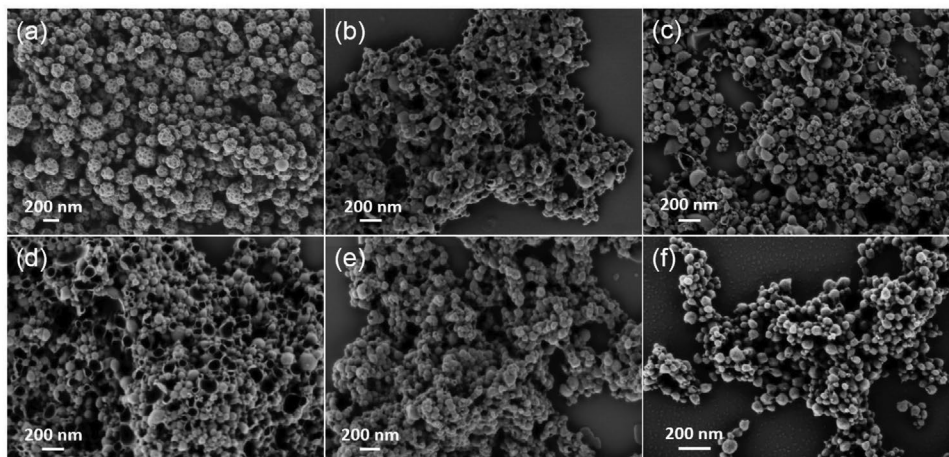
SiO$_2$ NCs with a tunable average hydrodynamic diameter ranging from 60 to 400 nm were synthesized. The other parameters were kept constant (Table S2, Supporting Information). As the oil/water volume ratio decreased from 40%, 20%, 10%, to 5%, the corresponding average hydrodynamic diameters decreased from 395, 147, 103, to 59 nm, respectively. All nanocapsules displayed well-defined core–shell structures, as shown by TEM in **Figure 3**. Increasing the concentration of the surfactant from 0.8 to 1.6 g L^{-1} led to remarkably small capsules with an average size of 45 nm (TEM micrographs in Figure S2, Supporting Information). The shell thickness can be increased by increasing the concentration of alkoxysilane in the dispersed phase and by controlling the ratio between oil and water. The corresponding shell thickness (d) are provided in Figure 3. As the hydrodynamic diameter of nanocapsule decreases from 395 to 59 nm, the shell thickness decreased accordingly from 17 to ≈ 4 nm.

2.3. Toward Bioinspired Compartmentalization

To generalize the nanocapsule formation for an effective loading of diverse payloads, a variety of hydrophobic liquids was used to form the core of SiO$_2$ NCs (Table S3, Supporting Information). Nanocapsules with defined core–shell structure

(**Figure 4**) and a diameter of ≈ 100–200 nm (Table S3, Supporting Information) were formed with various organic solvents. In the following study, we chose olive oil as a representative biocompatible solvent and chloroform as low boiling point solvent to form the core of NCs. In the latter case, chloroform could be evaporated after silica formation by diffusion through the aqueous continuous phase[43] and water filled the interior cavity of the NCs (Figure 1a). Thus, an oil–water core exchange process was carried out. Aqueous dispersions of water-filled nanocapsules were directly obtained in one pot, which mimics the biological cell membranes and intracellular compartments that display aqueous interiors. Usually, the synthesis of aqueous dispersions of nanocapsules with an aqueous core requires two steps: i) The capsule formation in inverse (water-in-oil) miniemulsions, and ii) the subsequent transfer in aqueous media and stabilization with an additional surfactant with high hydrophilic-lipophilic balance value. The organic solvent is evaporated afterward.[44,45]

The NCs prepared from olive oil and chloroform (the latter followed by solvent evaporation) here are denoted as NC$_{oil}$ and NC$_{water}$, respectively. The evaporation of chloroform was evidenced by the disappearance of its characteristic signal at 7.26 ppm in ^{1}H NMR spectra after 12 h (Figure S3, Supporting Information). As shown in **Figure 5**, a well-defined core–shell morphology of SiO$_2$ NCs was identified by TEM, indicating the successful condensation of alkoxysilane around the miniemulsion droplets. The average diameters determined in the dried state by scanning electron microscopy (SEM) were 34 ± 23 nm for NC$_{oil}$ and 58 ± 28 nm for NC$_{water}$. Their corresponding average shell thicknesses were 4.5 ± 1.8 and 4.4 ± 1.9 nm, as determined from TEM micrographs.

ADVANCED
SCIENCE NEWS
www.advancedsciencenews.com

Particle
& Particle Systems Characterization
www.particle-journal.com

Figure 4. SEM micrographs of SiO$_2$ NCs synthesized with different hydrophobic liquids as oil core: a) oleic triglyceride (sample SJP16-0), b) Miglyol 812N (sample SJP16-1), c) m-xylene (sample SJP1), d) hexadecane (sample SJP16-2), e) cyclohexane (sample SJP16-4), and f) dichloromethane (sample SJP82-0).

2.4. Controlled Release of Payloads

Site-specific release of drug molecules is the prime prerequisite for in vivo nanocarrier-mediated drug delivery. Controlled drug release can be achieved by preparing shells so that their permeability change in response to local conditions of target tissues. Here, we show that nanocapsules can be designed to selectively release the drug dexamethasone (DXM) in response to the presence of glutathione tripeptide (GSH). DXM is a hydrophobic glucocorticoid used to modulate the inflammatory response of liver macrophages. Systemic administration of glucocorticoids is associated with severe side-effects, such as hyperglycemia, hypertension, and intestinal bleeding.[46] Therefore, formulating DXM for its intracellular delivery and site-specific release
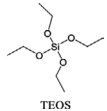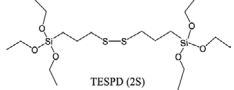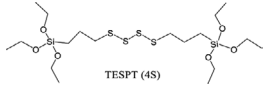
is necessary. The fact that glutathione-responsive nanocarriers can be used for targeted intracellular drug delivery is based on two aspects. i) Many therapeutics (e.g., anticancer drugs, such as doxorubicin and paclitaxel, photosensitizers, and antioxidants) and biotherapeutics (e.g., peptides, proteins, and siRNA) exert therapeutic effects only inside cells, such as cytosols or cell nuclei. ii) Some intracellular compartments, such as the cytosol, mitochondria, and cell nuclei contain a significantly higher concentration (about $2–10 \times 10^{-3}$ M) of glutathione tripeptides than their concentration in the extracellular and circulation fluids (about $2–20 \times 10^{-6}$ M).[47]

To this purpose, we introduced disulfide and tetrasulfide linkages into the silica shell of nanocapsules by using alkoxysilanes containing di-/tetrasulfide bonds as precursor for building the
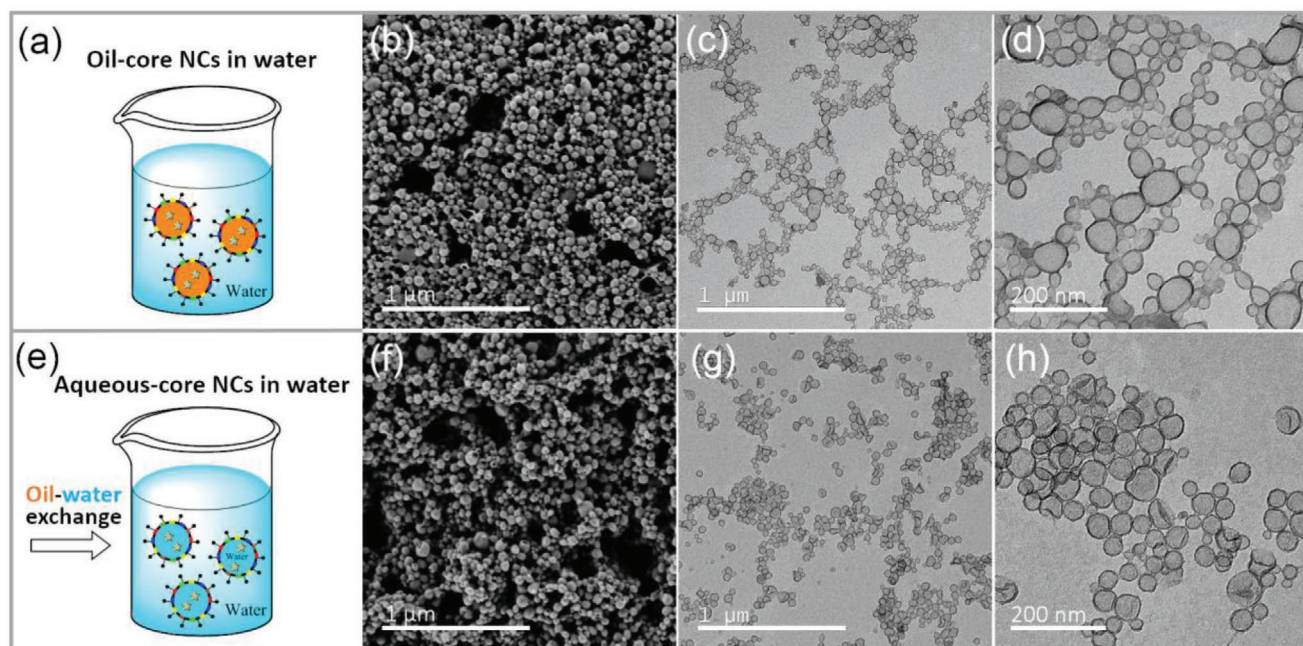
Figure 5. Scheme, SEM, and TEM micrographs of SiO$_2$ NC$_{oil}$ a–d) and NC$_{water}$ after the oil–water exchange process e–h).

Table 1. Hydrolysis degree of the emulsified alkoxysilanes, hydrodynamic diameters D_h, zeta potential ξ, and encapsulation efficiency of DXM after dialysis of the silica nanocapsules.

| Entry	Silica precursors	Content of Q_n and T_n sites [%][a]							D_h [nm]	ξ[b] [mV]	EE [%]
		Q_2	Q_3	Q_4	T_0	T_1	T_2	T_3			
NC$_{oil}$	TEOS	1	43	56	—	—	—	—	179 ± 53	−2 ± 1	38
NC$_{water}$		3	41	56	—	—	—	—	115 ± 55	−1 ± 1	39
NC$_{oil}$-2S-25%	TESPD (2S)	0	15	85	34	1	29	36	157 ± 54	−1 ± 1	58
NC$_{oil}$-2S-50%		0	15	85	76	2	10	12	169 ± 22	2 ± 1	60
NC$_{water}$-2S-25%		0	11	89	77	2	10	11	193 ± 38	−2 ± 1	45
NC$_{water}$-2S-50%		0	14	86	72	2	15	11	223 ± 118	−2 ± 1	—
NC$_{oil}$-4S-25%	TESPT (4S)	0	25	75	30	2	38	30	175 ± 74	1 ± 1	25
NC$_{water}$-4S-25%		0	14	86	64	2	27	7	210 ± 65	−4 ± 1	36

[a]Freeze-dried prior to the measurements; [b]Zeta potential of SiO$_2$ NCs stabilized by the nonionic surfactant Lutensol AT50.

silica shell. The resulting nanocapsules were denoted as SiO$_2$ NC-2S or SiO$_2$ NC-4S, respectively. In order to determine the amount of siloxane bridges, silanol groups, and incorporated disulfide and tetrasulfide linkages in the silica shell, the NC-2S/4S shells were measured by ^{29}Si MAS NMR and ^{13}C CP-MAS NMR spectroscopy. The ^{29}Si NMR spectra show signals at −110 and −100 ppm corresponding to the Q^4 and Q^3 units (Qn: Si(OSi)$_n$(OH)$_{4−n}$), respectively (Figure S4, Supporting Information). The high percentage of Q^4 signal (Q^4 > 55% for control samples and Q^4 ≥ 85% for all hybrid capsules) confirmed the successful formation of silica network by siloxane bridges (**Table 1**). Compared with NC$_{oil}$, the percentage of Q^4 signal of NCs filled with water increased slightly, indicating that the alkoxysilanes were further hydrolyzed when the core was exchanged with water. Moreover, the percentage of Q^4 signal is also related to the permeability of the silica shell. When the Q^4 signal increased from 56% for control NCs to 85% for NC$_{oil}$-2S-25%, the encapsulation efficiency of DXM increased over 50% owing to the higher crosslinking degree of the silica shell. The absence of free (Q^0) and monoreacted alkoxysilane (Q^1), and very low resonance corresponding to Q^2 (1% for NC$_{oil}$ and 3% for NC$_{water}$) showed that the alkoxysilanes were efficiently reacted. The signals at −68 and −58 ppm originated from the T^3 and T^2 units of the alkoxysilanes containing sulfide groups (T^m: CSi(OSi)$_m$(OH)$_{3−m}$), respectively (Figure S4, Supporting Information). The T signals together with ^{13}C signals at 12.1, 23.3, and 41.8 ppm corresponding to the ^{1}C, ^{2}C, and ^{3}C in the series of Si-^{1}C-^{2}C-^{3}C-S-S-^{3}C-^{2}C-^{1}C-Si, respectively, proved the integration of the sulfide-containing alkoxysilanes within the SiO$_2$ shell, forming an organic–inorganic hybrid silsesquioxane framework. T^0 signal indicated uncondensed functional alkoxysilanes, probably due to their higher hydrophobicity compared with tetraethoxysilane (TEOS). To confirm this hypothesis, we incubated pure bis(triethoxysilylpropyl)disulfide in CTMA-Cl aqueous solution under experimental condition. After stirring at 500 rpm for 7 d, a strong T^0 signal (74% compared to T^n signals) was measured. In parallel, freeze-dried powder of the sample NC$_{water}$-2S-25% was extracted repeatedly with ethanol. By this washing step, T^0 signal of the sample was significantly reduced from 77% to 24% (Table S4 and Figure S4h, Supporting Information). Both experiments showed the partial conversion of functional alkoxysilanes under the experimental conditions. The size distribution and zeta potential of SiO$_2$ NCs after incorporating the functional alkoxysilanes are listed in Table 1. The NCs measured here were stabilized by the nonionic surfactant Lutensol AT50 and therefore their surface charges were close to neutral. As a comparison, SiO$_2$ NCs stabilized by a cationic surfactant CTMA-Cl were positively charged (e.g., zeta potential was +12 mV for SiO$_2$ NC$_{oil}$). In addition, nanocapsules synthesized with chloroform as solvent were uniform when TEOS was used as sole silica precursor (Figure 5f–h). The size and polydispersity of NCs increased as the content of functional alkoxysilanes bis(triethoxysilylpropyl) disulfide (TESPD) and bis[3-(triethoxysilyl) propyl] tetrasulfide (TESPT) increased from 0% to 50% (Figure S5, Supporting Information).

In vitro glutathione-responsive release of DXM from SiO$_2$ NCs was studied by incubating purified nanocapsules in an aqueous medium containing 10×10^{-3} M GSH, which is commonly used to mimic the reducing intracellular microenvironment.[18,48,49] The GSH-responsive release mechanism is shown in **Figure 6**a.

Dispersions of SiO$_2$ NCs were incubated in the absence of GSH for control experiments. As shown in Figure 6c, less than 5% DXM was released within 15 d for all NC$_{oil}$-2S/4S. In the presence of GSH in the incubation medium (10×10^{-3} M), the release of DXM from NC$_{oil}$-2S-25% was dramatically

1900484 (6 of 12)
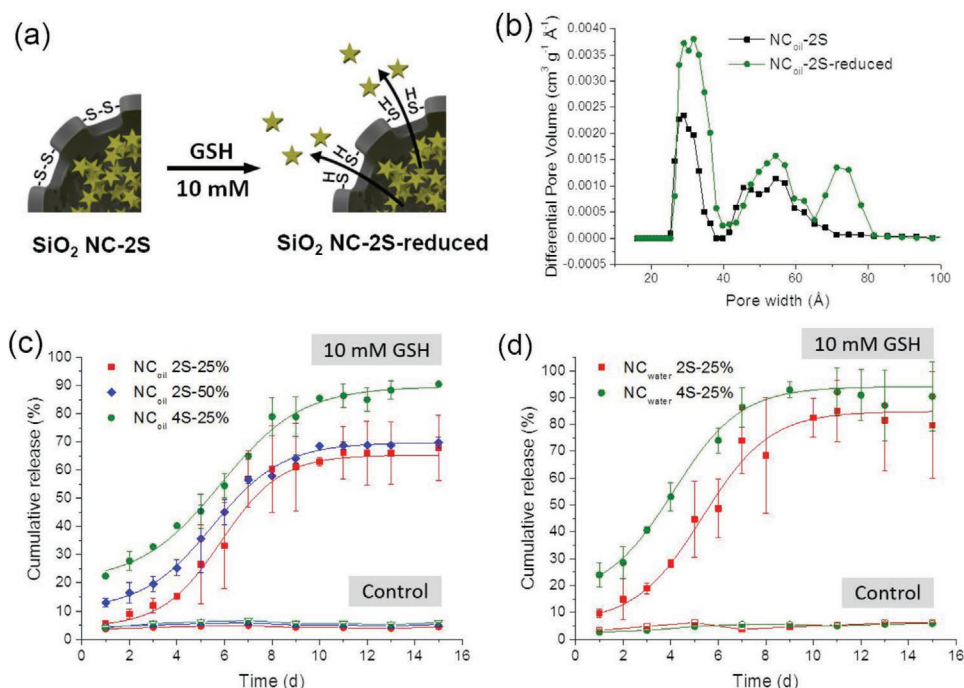
Figure 6. a) Schematic illustration of GSH-responsive release of DXM from SiO$_2$ NC-2S. b) Pore size distribution of SiO$_2$ NC-2S before and after reduction by GSH. Release profiles of DXM from c) SiO$_2$ NC$_{oil}$ and d) SiO$_2$ NC$_{water}$ containing various amounts of disulfide or tetrasulfide bonds in the shell. The open and solid symbols correspond to the samples incubated without (control) and with 10×10^{-3} M GSH in the medium, respectively. The DXM loading amount in the SiO$_2$ NCs was determined based on the encapsulation efficiency of DXM and the solid content of nanocapsule dispersions. The loading contents are 23.3 µg DXM mg^{-1} NC for SiO$_2$ NC$_{oil}$ 2S-25%, 16.6 µg mg^{-1} for SiO$_2$ NC$_{oil}$ 2S-50%, 6.0 µg mg^{-1} for SiO$_2$ NC$_{oil}$ 4S-25%, 20.2 µg mg^{-1} for SiO$_2$ NC$_{water}$ 2S-25%, and 13.7 µg mg^{-1} for SiO$_2$ NC$_{water}$ 4S-25%.

accelerated due to the cleavage of disulfide linkages that led to an increase of the permeability of the silica shell.[50] Both increasing the content of disulfide bonds or replacing disulfide by tetrasulfide bonds further increased the released amount of DXM at equilibrium (Figure 6c). No obvious differences were observed for the release profiles of nanocapsules with olive oil or water as the filling liquids (Figure 6c,d). Moreover, the GSH-responsive release profiles of DXM from SiO$_2$ NCs display a sigmoidal shape which is a unique feature and avoids the burst release of other release systems. Indeed, there were two diffusion processes taking place in the release system. First, GSH tripeptides are required to diffuse through the silica shell and cleave the disulfide linkages. Therefore, a relatively slow release was observed in the initial stage. As the amount of disulfide cleavage increased, the release was accelerated due to the increased permeability of the silica shell. This yields a sustained release of therapeutic payloads up to over 10 d.

The change in the permeability of the silica shell during the release process was investigated by nitrogen adsorption–desorption experiments. The pore size distribution of NC$_{oil}$-2S shifted to larger values due to the cleavage of disulfide linkages after incubation with 10×10^{-3} M GSH for 15 d (Figure 6b). Compared to NC$_{oil}$-2S before incubation, a new peak corresponding to pores with sizes ≈7–8 nm in width appeared for the reduced nanocapsules. The increase in the porosity of the silica shell after reduction is consistent with the specific release profiles of DXM in response to GSH. The core–shell structure was kept intact after release because the silica network formed

by silicium oxide bonds remain, while the disulfide bonds are opened.[25]

2.5. Control of Nanocapsule Functionalization

The core–shell structure allows flexible functionalization of nanocapsules by postfunctionalizing the outer surface, incorporating functional building blocks in precursors forming the shell, or via encapsulation in the interior cavity. Fluorescent dye Cyanine5 (Cy5) was covalently integrated in the silica shell by copolymerization. The presence of the dye is important for quantifying cellular uptake of NCs in CD8$^+$ T-cells by flow cytometry and visualizing the cell uptake process under confocal laser scanning microscopy (cLSM). After 24 h incubation, SiO$_2$ NCs showed good biocompatibility toward T-cells at nanocapsule concentrations up to 80 µg mL^{-1} (**Figure 7**a). Over 90% cells were Cy5 positive cells at NC concentration from 20 to 80 µg mL^{-1}, indicating a good cellular uptake of NCs by CD8$^+$ T-cells (Figure 7b). NCs were colocalized with lysosomes (Figure 7c–f), which is a solid proof of cellular uptake. High cell viability and uptake were also found for Jurkat and Hela cells as shown in Figures S6 and S7 (Supporting Information).

TEM provides higher resolution imaging for investigating cellular uptake and intracellular trafficking of nanocarriers. However, core–shell nanocapsules have a size and morphology that are similar to cellular organelles. Therefore, both types of compartments are difficult to distinguish. To overcome
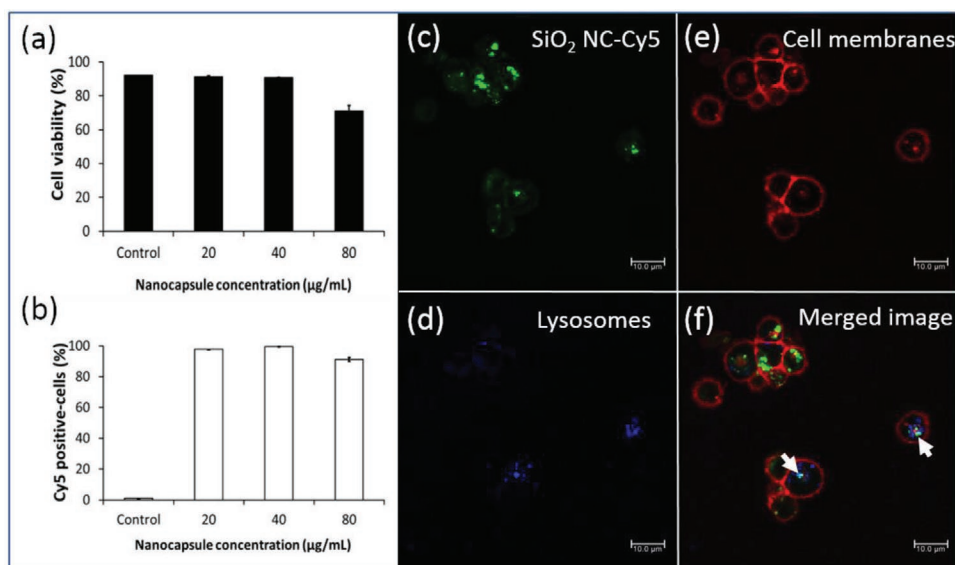
Figure 7. Cellular uptake study of Cy5-labeled SiO$_2$ NCs in CD8$^+$ T-cells. a) Cell viability and b) Cy5 positive-cells of CD8$^+$ T-cells after treatment with various concentrations of SiO$_2$ NCs for 24 h. cLSM images showing the cellular uptake of SiO$_2$ NCs and colocalization with lysosome in CD8$^+$ T-cells. c) The SiO$_2$ NCs were labeled with Cy5 (green), d) lysosomes were stained with LysoTracker Green DND-26 (blue), and e) the cell membranes were stained with CellMask Orange (red). f) The merged images of the three channels demonstrated that the NCs were colocalized with lysosomes, as indicated with white arrows.

this issue, we loaded SiO$_2$ NCs with iron oxide nanoparticles (Fe$_3$O$_4$ NPs), which provided a higher contrast and also allowed the localization of NCs by monitoring elemental distribution of silicon and iron. As shown in the TEM micrographs in **Figure 8**a–c, various amounts of iron oxide can be encapsulated in NCs (Table S5, Supporting Information). By encapsulating Fe$_3$O$_4$ NPs as contrast agent, SiO$_2$ NCs were clearly distinguished from cellular organelles (**Figure 9**). Combined with elemental mapping of silicon and iron obtained by electron energy loss spectroscopy (EELS, Figure 9c) and energy dispersive X-ray spectroscopy (EDS, Figure 9d), cellular uptake of nanocapsules and their localization in intracellular environment were successfully confirmed (Figure 9e). Superparamagnetism of Fe$_3$O$_4$ NPs was preserved after the encapsulation, with a saturated magnetization of 10.0 emu g^{-1} nanocapsules (Figure 8d). Therefore, the magnetic NCs are also potentially useful for magnetic resonance imaging and magnetic-guided targeted delivery.

3. Conclusions

We demonstrated here a versatile one-step synthesis of SiO$_2$ NCs for biomedical applications. This approach is based on a sol–gel process confined at the interface of oil-in-water miniemulsion droplets. Hydrodynamic diameters of NCs could be controlled between 60 and 400 nm. NCs are formed with various hydrophobic liquids for potentially encapsulating cargos with different solubility. Solvents with low boiling point can be evaporated to convert the interior cavity to an aqueous environment in one pot. By introducing disulfide or tetrasulfide bonds in the shell, the SiO$_2$ NCs show a specific and sustained release of dexamethasone in response to the presence of glutathione tripeptide for over 10 d. Fluorescent and magnetic

labeling enable monitoring of cellular uptake and intracellular trafficking of the NCs by fluorescence microscopy and TEM combined with elemental mapping. These features show that the versatile synthetic approach is promising for the controlled preparation of functional SiO$_2$ NCs for drug delivery applications.

4. Experimental Section

Materials: TEOS (Alfa Aesar, 98%), TESPD (Gelest, 90%), (TESPT, Sigma-Aldrich, 90%), 3-aminopropyltrimethoxysilane (APTES, Alfa Aesar, >98%), hexadecane (Sigma-Aldrich, 99%), olive oil (Sigma-Aldrich, highly refined, low acidity), oleic triglyceride (Sigma-Aldrich, ≥99%), Miglyol 812N (IOI Oleo), *m*-xylene (Sigma-Aldrich, ≥99%), cyclohexane (Sigma-Aldrich, 99.5%), chloroform (Sigma-Aldrich, ≥99%), dichloromethane (Sigma-Aldrich, ≥99.8%), cetyltrimethylammonium chloride (CTMA-Cl, Acros Organics, 99%), Lutensol AT50 (BASF), DXM (Sigma-Aldrich, ≥98%), and GSH (Appli Chem, ≥97%) were used as received. Amine-reactive fluorescent dye Cyanine5 NHS ester (Cy5-NHS) was purchased from Lumiprobe GmbH, Germany. Oleic acid capped iron oxide nanoparticles (Fe$_3$O$_4$ NPs) were synthesized by a standard co-precipitation protocol.[51] Milli-Q water was used throughout the synthesis and purification processes of SiO$_2$ NCs.

Synthesis of Silica Nanocapsules: Silica nanocapsules were synthesized in an oil-in-water miniemulsion by using the surface of oil nanodroplets as template for the hydrolysis and condensation of alkoxysilanes. Specifically, 2.0 g (9.6 mmol) of TEOS was first mixed with 125 mg of hexadecane and 1 g of organic solvent to form the oil phase. Drug (50 mg of DXM, equals to 1.67 mg mL^{-1} in the dipersion) or iron oxide nanoparticles can be dissolved or dispersed in the organic solvent and subsequently will be encapsulated in the core of nanocapsules. In the second step, 30 mL of 0.77 mg mL^{-1} aqueous solution of CTMA-Cl was poured into the oil mixture under stirring. After a pre-emulsification step by stirring at 1000 rpm for 1 h, the obtained emulsion was sonicated by using a Branson 450 W sonifier with a 1/2″ tip at 70% amplitude for 180 s (30 s of sonication, 10 s of pause) with ice cooling. The resulting miniemulsion was stirred at 1000 rpm for 12 h at room temperature to
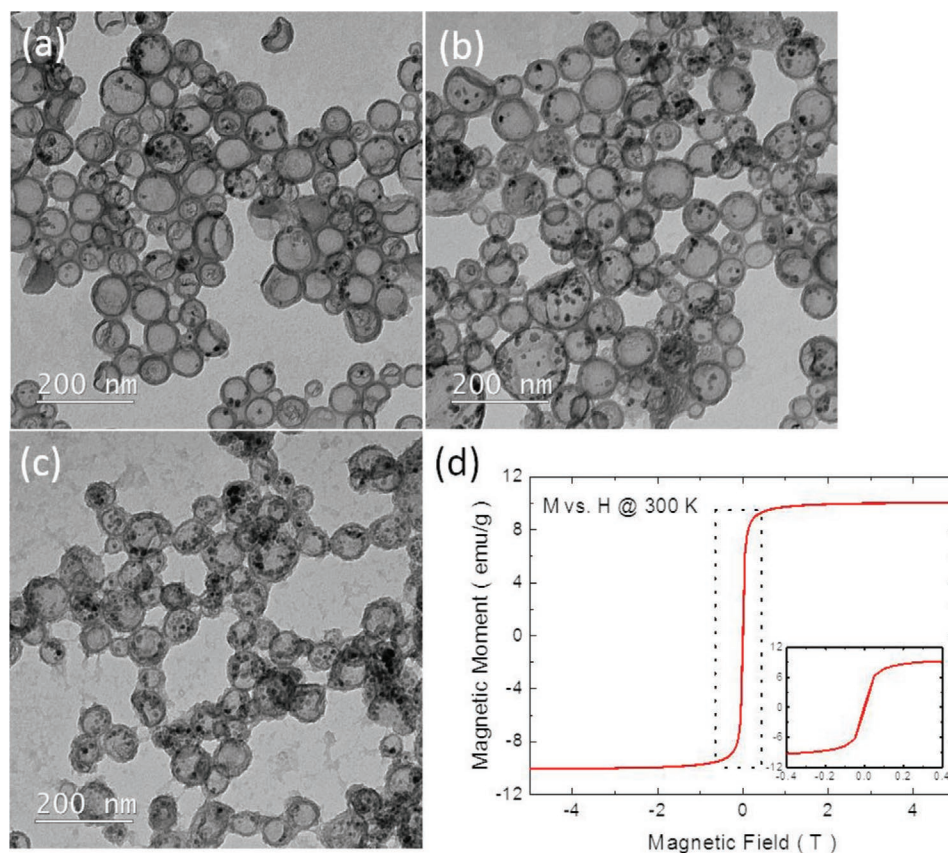
Figure 8. Characterization of SiO$_2$ NCs loaded with various amounts of iron oxide nanoparticles. TEM micrographs of NCs with $m_{\text{iron oxide}}$:m_{silica} = a) 1:6.2 (sample SJP29-2), b) 1:2.8 (sample SJP29-3), and c) 1:1.7 (sample SJP29-4). d) VSM magnetization curve of NCs with $m_{\text{iron oxide}}$:m_{silica} = 1:2.8.
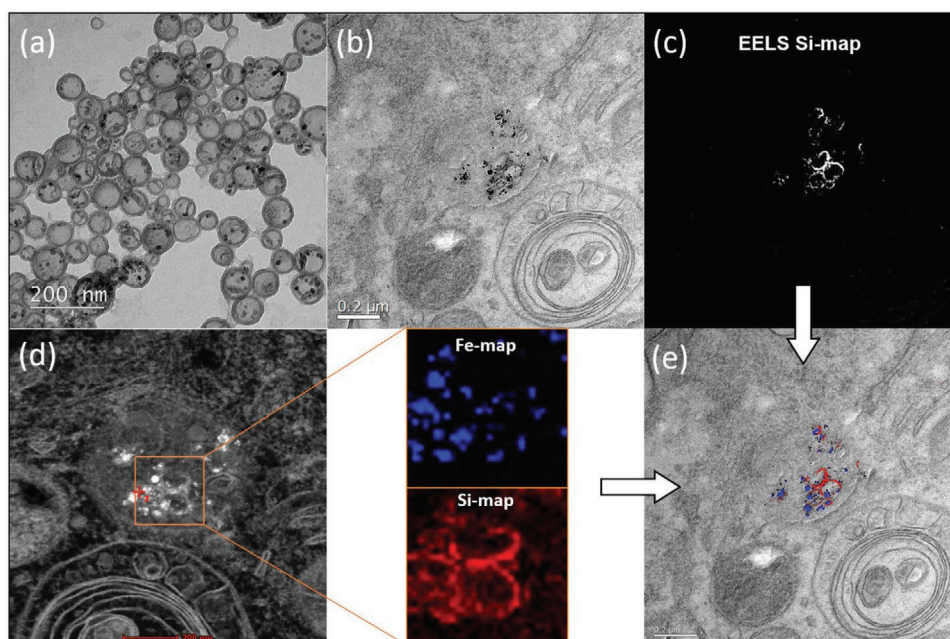
Figure 9. Intracellular localization of SiO$_2$ NCs labeled with Fe$_3$O$_4$ NPs in Hela cells by TEM and elemental mapping. TEM micrographs of a) SiO$_2$ NCs containing Fe$_3$O$_4$ NPs, b) NCs in cells, c) elemental mapping of silicon obtained by EELS, d) elemental mapping of silicon and iron obtained by EDS, e) colocalization of NCs based on TEM, EELS, and EDS data.

1900484 (9 of 12)

obtain an aqueous dispersion of SiO$_2$ NCs. For NCs using chloroform as the core liquid, the dispersions were further stirred at 1000 rpm for another 12 h without the lids for the vials in order to evaporate the chloroform and achieve oil–water exchange for the interior of NCs. In the case of nanocapsules containing disulfide or tetrasulfide linkages in the shell, a certain amount of TEOS and TESPD/TESPT (in total 9.6 mmol) were used as alkoxysilane precursors. For the fluorescent labeling of SiO$_2$ NCs, Cy5-NHS was first coupled with APTES at a molar ratio of 1:1.1 to obtain fluorescently labeled silica precursors. The APTES-Cy5 conjugates were then mixed with TEOS as the silica source. The molar ratio of Cy5 with TEOS was 1:14 000.

Encapsulation Efficiency of DXM: SiO$_2$ NCs were PEGylated by exchanging the templating surfactant CTMA-Cl with the nonionic surfactant Lutensol AT50. PEGylated nanocapsules were denoted as SiO$_2$ NC-PEG. Specifically, 35 mg of Lutensol AT50 was added to 2 mL of SiO$_2$ NCs dispersion. The dispersion was stirred at 1000 rpm for 2 h and then dialyzed against water with a dialysis tube with molecular weight cut-off (MWCO) of 1000 g mol^{-1}. In this case, CTMA-Cl (M_w = 320 g mol^{-1}) could diffuse through the dialysis membrane into the aqueous dialysis medium, while Lutensol AT50 (M_w = 2460 g mol^{-1}) was kept inside. During the dialysis, the encapsulation efficiency of DXM in NCs was determined. The dialysis medium was changed three times per day until no DXM could be detected in the supernatant. The concentration of nonencapsulated DXM was determined by UV–vis spectroscopy (λ_{max} = 243 nm). The encapsulation efficiency of DXM in NCs was expressed as the percentage of encapsulated DXM with respect to the initial amount of DXM. The calibration curve for the determination of DXM in water is shown in Figure S8 (Supporting Information). Afterward, the dialyzed dispersion was centrifuged at 10 k rpm to remove the excess of Lutensol AT50. The pellet was redispersed in water and the dispersion was stirred at 1000 rpm for 24 h.

Glutathione-Responsive Molecular Release from Silica Nanocapsules: Stimuli-responsive molecular release from SiO$_2$ NCs was performed by dialysis (MWCO of 14 kDa for the membranes). First, 0.3 mL of NC dispersion and 0.7 mL of water were placed in a dialysis tube, which was then immersed in 30 mL of dialysis medium containing 10×10^{-3} M of glutathione. Milli-Q water was used as release medium in control experiments. The dialysis system was incubated at 37 °C in a HLC thermomixer (MKR 23, Pforzheim, Germany). The concentration of released DXM was determined by UV–vis spectroscopy by taking 0.5 mL of supernatant from the incubation medium at given intervals. An equal volume of fresh incubation medium was added to the release media. The release profile of DXM was expressed as cumulative percentage of released drug compared to the initial amount of loaded DXM, while the effect of dilution was taken into account. The drug release experiments were performed in triplicate for each sample.

Cellular Uptake Study by Flow Cytometry: CD8$^+$ T-cells resuspended in RPMI cell culture medium containing 1% fetal bovine serum (FBS) and 100 U mL^{-1} IL-2 without antibiotics were added into 0.1 µg mL^{-1} of anti-CD3 immobilized 24-well plate at a density of 200 000 cells per well. Then, various concentrations of SiO$_2$ NCs were incubated with the cells for 24 h. After that, the cells were washed and resuspended in PBS. Flow cytometry measurements were performed on a Attune NxT Flow Cytometer (Invitrogen, USA). Zombie Aqua dye (BioLegend, USA) was used for live cell indicating with the excitation of the violet laser (405 nm) and detected in channel VL-2. Cy5 dye labeled NCs were excited with red laser (638 nm) and recorded in channel RL-1. Data analysis was performed using Attune NxT software (Invitrogen, USA) by selecting the cells on a forward/sideward scatter plot, thereby excluding cell debris. These gated events were shown by the histogram of fluorescent signal. Percentages of cell viability were recorded from living cells (Zombie Aqua negative-cells) compared to dead cells (Zombie Aqua positive-cells). After gating for living cells, the cells that supposed to take up the SiO$_2$ NCs containing Cy5 dye were reported as Cy5 positive-cells.

Cell Imaging by cLSM: To confirm the cellular uptake, CD8$^+$ T-cells were treated with the SiO$_2$ NCs as describe above. After that, the cells were washed and transferred to µ–Slide 8 well with a glass coverslip bottom (Ibidi, Germany). Live cell images were taken with

a commercial setup (LSM SP5 STED Leica Laser Scanning Confocal Microscope, Leica, Germany), consisting of an inverse fluorescence microscope DMI 6000 CS equipped with a multilaser combination, five detectors operating in the range of 400–800 nm. A HCX PL APO CS 63 × 1.4 oil objective was used in this study. LysoTracker Green DND-26 (50 × 10^{-9} M diluted in Dulbecco's modified Eagle's medium, Life Technologies, USA) was used to stain lysosome for 1 h, excited with an Ar laser (488 nm), detected at 510–540 nm and pseudocolored in blue. The membrane was stained with CellMaskOrange and pseudocolored in red. The SiO$_2$ NCs was labeled with Cy5 and pseudocolored in green. The merged images of three channels demonstrated that the Cy5 labeled SiO$_2$ NCs were colocalized with lysosomes as indicated with white arrows.

TEM Analysis: Sapphire disks (3 mm; M. Wohlwend GmbH) were precoated with a 10 nm thick carbon layer using an EM MED020 instrument (Leica). The coated sapphire disks were dried and sterilized in an oven at 120 °C overnight before use. HeLa cells were seeded onto sapphire disks in 12-well plates overnight for cell attachment. SiO$_2$ NCs (loaded with Fe$_3$O$_4$ NPs) were incubated with Hela Cells at 75 µg mL^{-1} for 2 h, 10 h, and overnight in a humidified incubator at 37 °C and 5% CO$_2$. After the incubation, each sapphire disk was collected from the 12-well plates and slightly immersed into 1-hexadecene before placing them between two aluminum plates (3 mm, Plano). This "sandwich" structure was placed into a specimen holder for high pressure freezing in a Wohlwend HPF Compact 01 high pressure freezer with a pressure of 2100 bar for 2–3 s. The specimen holder was withdrawn from the freezer and immersed into liquid nitrogen to release the sample. The frozen sample was then labeled and stored in a container filled with liquid nitrogen. Subsequently, freeze substitution of the sample was carried out in a 0.5 mL Eppendorf tube using an AFS2 automated freeze substitution device (Leica). Each tube contained 1 mL of freeze substitution solution, consisting of 0.2 wt/vol% osmium tetroxide, 0.1 wt/vol% uranyl acetate, and 5% distilled water in acetone. The tubes were first kept at −90 °C and slowly warmed up to 0 °C in 24 h. After keeping at room temperature for 1 h, the substitution solution was removed and the samples were washed 3 times with acetone. Each sample was infiltrated in an ascending epoxy resin series (30%, 50%, and 75% in acetone) for 1 h before finally infiltration in 100% epoxy resin overnight. Finally, each sample was transferred into a new Eppendorf tube containing freshly prepared pure epoxy resin for polymerization at 60 °C for 24 h. After polymerization, sample blocks were kept at room temperature until their sectioning. Sample blocks for each time point were trimmed and sectioned into 100 nm sections by a 45° diamond knife (Diatome) in EM UC6 ultramicrotome (Leica). Sections were then carefully placed onto 300-mesh copper grid for standard bright-field, EELS, and EDS analysis in Tecnai F20 200 kV TEM (FEI). Bright-field TEM micrographs were obtained with a Gatan US1000 2k CCD camera. EDX images were collected with an EDAX detector.

Characterization of Nanocapsules: Hydrodynamic diameters of SiO$_2$ NCs were measured by dynamic light scattering with a Nicomp particle sizer (Model 380, PSS, Santa Barbara, CA) at a fixed scattering angle of 90°. The morphology of nanocapsules was examined with a Gemini 1530 (Carl Zeiss AG, Oberkochem, Germany) SEM operating at 0.35 kV and a Jeol 1400 (Jeol Ltd, Tokyo, Japan) transmission electron microscope operating at an accelerating voltage of 120 kV. SEM and TEM samples of nanocapsules were prepared by casting the diluted dispersions on silicon wafers and carbon layer-coated copper grids, respectively. Surface area of nanocapsules was determined from nitrogen adsorption– desorption experiments carried out on a Quantachrome Autosorb-1 analyzer (Boynton Beach, FL) at 77.3 K. The capsule dispersions were dialyzed against Milli-Q water for 3 d to remove the surfactant. The dialyzed dispersions were then freeze-dried for 48 h and degassed at 70 °C under high vacuum for at least 12 h before measurements. The specific surface area was calculated using the Brunauer–Emmett–Teller equation based on data points obtained from $0 < P/P_0 < 0.25$. Zeta potential measurements were performed in 10^{-3} M potassium chloride solution at pH 6.8 and 25 °C with a Malvern Zeta sizer (Malvern Instruments, UK). Solid content of the capsule dispersion was measured

gravimetrically. Quantitative ^{29}Si MAS-NMR spectra were recorded with a Bruker Avance II spectrometer operating at 300.23 MHz ^{1}H Larmor frequency using a commercial double resonance MAS probe supporting MAS rotors with 7 mm outer diameter. Direct excitation spectra were acquired with a small excitation angle of $\approx 20°$ at 25 kHz rf-nutation frequency and 60 s relaxation delay between subsequent transients. In order to avoid line broadening due to dipolar couplings, SPINAL64 hetero-nuclear decoupling at 50 kHz rf-nutation frequency has been applied.[52] Typically, 1600–2000 transients with 4096 data points and 20 μs dwell time have been recorded. The ^{29}Si NMR signals were referenced to tetrakis(trimethylsilyl)silane[53] and the assignments of $T^{(n)}$ and $Q^{(n)}$ groups were taken from the literature.[54] The content of $T^{(n)}$ and $Q^{(n)}$ groups was quantified via deconvolution of the ^{29}Si MAS-NMR spectra using the DMfit program by Massiot et al.,[55] because the overlapping NMR signals of different $T^{(n)}$ and $Q^{(n)}$ groups could not be quantified by integration.

Conflict of Interest

The authors declare no conflict of interest.

[1] R. Kannan, E. Nance, S. Kannan, D. A. Tomalia, *J. Intern. Med.* **2014**, *276*, 579.

[2] J. D. Heidel, M. E. Davis, *Pharm. Res.* **2011**, *28*, 187.

[3] T. Lammers, F. Kiessling, W. E. Hennink, G. Storm, *J. Controlled Release* **2012**, *161*, 175.

[4] A. Z. Wang, R. Langer, O. C. Farokhzad, *Annu. Rev. Med.* **2012**, *63*, 185.

[5] J. Xie, S. Lee, X. Chen, *Adv. Drug Delivery Rev.* **2010**, *62*, 1064.

[6] S. M. Janib, A. S. Moses, J. A. MacKay, *Adv. Drug Delivery Rev.* **2010**, *62*, 1052.

[7] R. Bardhan, S. Lal, A. Joshi, N. J. Halas, *Acc. Chem. Res.* **2011**, *44*, 936.

[8] T. Lammers, S. Aime, W. E. Hennink, G. Storm, F. Kiessling, *Acc. Chem. Res.* **2011**, *44*, 1029.

[9] D. Yoo, J.-H. Lee, T.-H. Shin, J. Cheon, *Acc. Chem. Res.* **2011**, *44*, 863.

[10] J. Kim, Y. Piao, T. Hyeon, *Chem. Soc. Rev.* **2009**, *38*, 372.

[11] Z. Li, J. C. Barnes, A. Bosoy, J. F. Stoddart, J. I. Zink, *Chem. Soc. Rev.* **2012**, *41*, 2590.

[12] P. Yang, S. Gai, J. Lin, *Chem. Soc. Rev.* **2012**, *41*, 3679.

[13] I. I. Slowing, J. L. Vivero-Escoto, C.-W. Wu, V. S. Y. Lin, *Adv. Drug Delivery Rev.* **2008**, *60*, 1278.

[14] A. Maity, V. Polshettiwar, *ChemSusChem* **2017**, *10*, 3866.

[15] F. Tang, L. Li, D. Chen, *Adv. Mater.* **2012**, *24*, 1504.

[16] D. Wibowo, Y. Hui, A. P. J. Middelberg, C.-X. Zhao, *Adv. Colloid Interface Sci.* **2016**, *236*, 83.

[17] D. Wang, Z. Xu, Z. Chen, X. Liu, C. Hou, X. Zhang, H. Zhang, *ACS Appl. Mater. Interfaces* **2014**, *6*, 12600.

[18] M. Zhou, X. Du, W. Li, X. Li, H. Huang, Q. Liao, B. Shi, X. Zhang, M. Zhang, *J. Mater. Chem. B* **2017**, *5*, 4455.

[19] P. Huang, Y. Chen, H. Lin, L. Yu, L. Zhang, L. Wang, Y. Zhu, J. Shi, *Biomaterials* **2017**, *125*, 23.

[20] A. Burns, H. Ow, U. Wiesner, *Chem. Soc. Rev.* **2006**, *35*, 1028.

[21] H. Ow, D. R. Larson, M. Srivastava, B. A. Baird, W. W. Webb, U. Wiesner, *Nano Lett.* **2005**, *5*, 113.

[22] F.-P. Chang, Y. Hung, J.-H. Chang, C.-H. Lin, C.-Y. Mou, *ACS Appl. Mater. Interfaces* **2014**, *6*, 6883.

[23] F. P. Chang, Y. P. Chen, C. Y. Mou, *Small* **2014**, *10*, 4785.

[24] S. Jiang, L. Lv, Q. Li, J. Wang, K. Landfester, D. Crespy, *Nanoscale* **2016**, *8*, 11511.

[25] S. Jiang, K. Landfester, D. Crespy, *RSC Adv.* **2016**, *6*, 104330.

[26] J. Fickert, P. Rupper, R. Graf, K. Landfester, D. Crespy, *J. Mater. Chem.* **2012**, *22*, 2286.

[27] D. Wibowo, C.-X. Zhao, A. P. Middelberg, *Chem. Commun.* **2014**, *50*, 11325.

[28] K. Qian, T. Shi, S. He, L. Luo, X. Liu, Y. Cao, *Microporous Mesoporous Mater.* **2013**, *169*, 1.

[29] K. Hayashi, M. Nakamura, K. Ishimura, *Chem. Commun.* **2011**, *47*, 1518.

[30] S. Jiang, B. C. Ma, J. Reinholz, Q. Li, J. Wang, K. A. Zhang, K. Landfester, D. Crespy, *ACS Appl. Mater. Interfaces* **2016**, *8*, 29915.

[31] M. Ma, F. Yan, M. Yao, Z. Wei, D. Zhou, H. Yao, H. Zheng, H. Chen, J. Shi, *ACS Appl. Mater. Interfaces* **2016**, *8*, 29986.

[32] L. Sun, Y. Zang, M. Sun, H. Wang, X. Zhu, S. Xu, Q. Yang, Y. Li, Y. Shan, *J. Colloid Interface Sci.* **2010**, *350*, 90.

[33] H. Chen, J. He, H. Tang, C. Yan, *Chem. Mater.* **2008**, *20*, 5894.

[34] P. W. Latham, *Nat. Biotechnol.* **1999**, *17*, 755.

[35] D. Wibowo, C.-X. Zhao, A. P. J. Middelberg, *Langmuir* **2015**, *31*, 1999.

[36] A. Jakhmola, R. Vecchione, D. Guarnieri, V. Belli, D. Calabria, P. A. Netti, *Adv. Healthcare Mater.* **2015**, *4*, 2688.

[37] P. Erni, G. Dardelle, M. Sillick, K. Wong, P. Beaussoubre, W. Fieber, *Angew. Chem.* **2013**, *125*, 10524.

[38] M. Hans, A. Lowman, *Curr. Opin. Solid State Mater. Sci.* **2002**, *6*, 319.

[39] A. P. Philipse, M. P. Van Bruggen, C. Pathmamanoharan, *Langmuir* **1994**, *10*, 92.

[40] K. Landfester, *Macromol. Rapid Commun.* **2001**, *22*, 896.

[41] N. Hoshyar, S. Gray, H. Han, G. Bao, *Nanomedicine* **2016**, *11*, 673.

[42] K. Landfester, *Annu. Rev. Mater. Res.* **2006**, *36*, 231.

[43] R. H. Staff, D. Schaeffel, A. Turshatov, D. Donadio, H. J. Butt, K. Landfester, K. Koynov, D. Crespy, *Small* **2013**, *9*, 3514.

[44] D. Crespy, M. Stark, C. Hoffmann-Richter, U. Ziener, K. Landfester, *Macromolecules* **2007**, *40*, 3122.

[45] R. Dorresteijn, N. Billecke, M. Schwendy, S. Pütz, M. Bonn, S. H. Parekh, M. Klapper, K. Müllen, *Adv. Funct. Mater.* **2014**, *24*, 4026.

[46] L. W. Doyle, R. A. Ehrenkranz, H. L. Halliday, *Neonatology* **2010**, *98*, 217.

[47] R. Cheng, F. Feng, F. Meng, C. Deng, J. Feijen, Z. Zhong, *J. Controlled Release* **2011**, *152*, 2.

[48] J. F. Quinn, M. R. Whittaker, T. P. Davis, *Polym. Chem.* **2017**, *8*, 97.

[49] C. Yang, W. Guo, L. Cui, N. An, T. Zhang, G. Guo, H. Lin, F. Qu, *J. Mater. Chem. B* **2015**, *3*, 1010.

[50] J. Fickert, D. Schaeffel, K. Koynov, K. Landfester, D. Crespy, *Colloid Polym. Sci.* **2014**, *292*, 251.

[51] M. B. Bannwarth, S. W. Kazer, S. Ulrich, G. Glasser, D. Crespy, K. Landfester, *Angew. Chem., Int. Ed.* **2013**, *52*, 10107.

[52] B. Fung, A. Khitrin, K. Ermolaev, *J. Magn. Reson.* **2000**, *142*, 97.

[53] H. Marsmann, W. Raml, E. Hengge, *Z. Naturforsch. B* **1980**, *35*, 1541.

[54] G. Engelhardt, D. Michel, *High-Resolution Solid-State NMR of Silicates and Zeolites*, John Wiley & Sons, Chichester, New York, Brisbane, Toronto, Singapore **1987**.

[55] D. Massiot, F. Fayon, M. Capron, I. King, S. Le Calvé, B. Alonso, J. O. Durand, B. Bujoli, Z. Gan, G. Hoatson, *Magn. Reson. Chem.* **2002**, *40*, 70.